AsPac J. Mol. Biol. Biotechnol. 2024
Vol. 32 (2) : 1-14

Bacterial nanocellulose (BNC) biosynthesis by *Komagataeibacter hansenii* RM-03 using agricultural waste as substrates and BNC-silver nanocomposite preparation

Aini Darwina Daud[a], Nor'Aini Abdul Rahman[a,b], Hooi Ling Foo[a] and Rosfarizan Mohamad[a,b*]

[a]*Department of Bioprocess Technology, Faculty of Biotechnology and Biomolecular Sciences, Universiti Putra Malaysia, 43400, UPM Serdang, Selangor, Malaysia.*
[b]*Bioprocessing and Biomanufacturing Research Complex, Faculty of Biotechnology and Biomolecular Sciences, Universiti Putra Malaysia, 43400, UPM Serdang, Selangor, Malaysia.*

Received 26th May 2023 / Accepted 29th January 2024 / Published 1st April 2024

Abstract. Bacterial nanocellulose (BNC) is a remarkable biopolymer synthesised by bacterium, exhibiting exceptional properties. However, conventional Hestrin-Schramm (HS) medium, particularly the carbon source, poses challenges of high costs and low productivity. This study explores BNC biosynthesis on a modified HS medium, employing agricultural wastes (sugarcane molasses, banana peel, and pineapple peel) as carbon sources, and compares the overall yield of BNC produced. Sugarcane molasses proved to be the most effective, yielding the highest BNC concentration (8.19 g/L) after 7 days, followed by pineapple peel (2.16 g/L) and banana peel (2.11 g/L). Extensive research was conducted to enhance properties of BNC by an environmentally friendly approach, incorporating silver nanoparticles (AgNP) utilising *Momordica charantia* fruit extract, resulting in a BNC-Ag nanocomposite. The synthesis involved mixing 1 mM silver nitrate ($AgNO_3$) with 15 mL of *M. charantia* fruit extract to reduce Ag ions to AgNP, which was confirmed by UV-vis spectroscopy with an absorbance peak between 400 and 410 nm. Characterisation using FESEM and TEM on the synthesized BNC showed minimal impact on BNC fiber diameter from waste-derived carbon sources. XRD indicated slight variations in crystallinity index, with the highest (85%) in TSM-derived BNC. FTIR analysis revealed similar chemical profiles across all BNC, indicating cellulose formation. The BNC-Ag nanocomposite exhibited potent antibacterial activity against multi-drug resistant strains (*Pseudomonas aeruginosa, Salmonella typhi, Bacillus subtilis, Staphylococcus aureus*) through disc diffusion method with inhibition zones up to 16.8 mm. Overall, the findings from this study contribute to the development of environmentally sustainable for the production of functional BNC materials with enhanced properties for diverse applications.

Keywords: agricultural wastes, bacterial nanocellulose, *Komagataeibacter hansenii*, *Momordica charantia*, silver nanoparticle

INTRODUCTION

Nanocellulose, a product derived from cellulose, having dimensions ranging from 1 nm to 100 nm, as defined by the International Organization for Standardization (ISO, 2023). It has excellent properties over native cellulose such as high surface area, high mechanical strength, good biodegradability and good biocompatibility due to its nano-scaled structure (Trache *et al.*, 2020). However, obtaining nanocellulose from plant sources like wood pulp and agricultural waste is complex as it requires chemically and mechanically induced treatment to remove non-cellulosic materials (Lin and Dufresne, 2014). This process yields cellulose nanocrystals (CNCs) and cellulose nanofibrils (CNFs), respectively. Alternative way to obtain pure nanocellulose directly is from bacteria, known as bacteria nanocellulose (BNC). BNC offers a simpler and

* Author for correspondence: Rosfarizan Mohamad, Faculty of Biotechnology and Biomolecular Sciences, Universiti Putra Malaysia, Malaysia
Email – farizan@upm.edu.my

eco-friendly way to make nanocellulose as it uses less energy and controlled processes during synthesis (Yahya *et al.,* 2023).

The process by which BNC is made involves the conversion of glucose to cellulose in four main steps: first, glucokinase phosphorylates glucose to glucose-6-phosphate; next, phosphoglucomutase isomerizes glucose to glucose-1-phosphate; next, UDP-glucose pyrophosphorylase transforms glucose to uridine diphosphate glucose (UDP-glucose) and finally, cellulose synthase produces cellulose. A three-dimensional network of nanofibres is created along the way as glucose chains are extruded out of bacterial cells, aggregated, and converted into cellulose ribbons (Ross *et al.,* 1991).

BNC is often biosynthesised by bacterial strains in Hestrin-Schramm (HS) medium which contains glucose, yeast extract, peptone, disodium hydrogen phosphate and citric acid. This medium is relatively expensive, and it limits the scale-up of BNC for industrial application for practical considerations (Jozala *et al.,* 2016). Nowadays, the use of agricultural wastes offers a way to overcome these problems by replacing HS medium either partially or entirely for the synthesis of BNC (Abol-Fotouh *et al.,* 2020). However, replacing entirely with agricultural wastes would result in an undefined medium, since the components would be variable. According to Zhang and Greasham (1999), a defined medium allows for better reproducibility, easier monitoring, and process control. Additionally, optimizing the medium requires consideration of the minimal growth requirements of the microorganisms (Singh *et al.,* 2017). Effectively competing against conventional mediums remains a challenge; nevertheless, formulating a medium by replacing expensive components with cheap sources stands out as a successful optimization strategy, besides the cost can also be reduced (Singh *et al.,* 2017).

Upon biosynthesis, BNC obtained directly from culture medium appears as a semi-transparent membrane made up almost entirely of water. Its exceptional water retention capability makes it valuable in applications like wound dressings where moisture retention is crucial. However, BNC alone lacks certain properties, including antibacterial activity. To enhance its functionalities, BNC is combined with other components, creating a valuable hybrid material. Previously, BNC nanocomposite was developed integrating silver nanoparticles (AgNP), leveraging the potent antibacterial properties of AgNP and the unique structural properties of BNC (Maneerung *et al*., 2008). Besides, given the rise of multidrug-resistant bacteria, there is a critical need for alternative antimicrobial materials. The formation of BNC-Ag nanocomposite offers a potential solution to combat these resistant strains. Additionally, BNC is highly beneficial, offering prolonged moisture retention, protection against infections, and improved exudates removal (Barja, 2021).

The synthesis of nanoparticles is typically carried out using silver nitrate ($AgNO_3$) as the precursor of silver and reducing agent such as sodium borohydride ($NaBH_4$), however the concerns with this method are the cost and toxicity (Zhang *et al*., 2016). In recent years, advancements in the green synthesis of AgNP using plant-assisted reduction have made it possible to replace the use of expensive reducing agents due to the naturally-presence of phytochemicals such as phenols, flavones, amides, terpenoids and ketones (Prabhu and Poulose, 2012). Several studies have reported on the use of plant extract, leaf extract and fruit extract as an *in situ* reducing agent to form AgNP (Krithiga *et al*., 2015; Masum *et al*., 2019; Naveed *et al*., 2022). To our knowledge, not many have reported on the incorporation of green-synthesised AgNP into BNC. Among the notable green assisted AgNP synthesisers, *Momordica charantia* (*M. charantia*) takes the spotlight, recognised not just for its abundance of phytochemicals but also for use in folk and traditional medicines due to exceptional biological properties, including anti-inflammatory, anti-microbial, and anticancer (Bortolotti *et al*., 2019; Dandawate *et al*., 2016). It is therefore of keen interest to investigate the ability of green-synthesised AgNP derived *M. charantia* fruit extract to form nanocomposite with BNC.

Thus, the primary objective of this study was to enhance the synthesis of BNC through the utilisation of hydrolysates derived from economically viable agricultural wastes, namely sugarcane molasses, banana peel, and pineapple peel, serving as substitutes for glucose in a conventional Hestrin-Schramm (HS) medium.

This approach aimed at achieving both sustainable and cost-effective BNC production. Subsequently, the synthesised BNC was further optimized for functional properties by incorporating AgNP, obtained from silver and *M. charantia* fruit extract, resulting in the formation of a BNC-Ag nanocomposite. Comprehensive characterisation of both pure BNC and the synthesised BNC-Ag nanocomposite included an examination of their morphology, structural, and functional group properties. Furthermore, the study also evaluated the antibacterial activity of the BNC-Ag nanocomposite, specifically targeting multi-drug resistant bacteria in addressing challenges associated with antibiotic resistance.

MATERIALS AND METHODS

Conversion of agricultural wastes into fermentable sugars solution

The fruit peel waste such as banana and pineapple were collected from a local stall at Serdang, Malaysia. All fruit peel waste was prepared according to Khan *et al.* (2021). The peels were washed and dried in an oven at room temperature for 72 h. About 250 g of the peels were ground to a fine paste using commercial dry miller, and immersed in 500 mL of distilled water separately. The mixtures were left at 90 °C for 60 min, and centrifuged at 2580 xg for 20 min. The supernatant was collected and labeled as BPW (banana peel waste) and PPW (pineapple peel waste) before being stored at 4 °C. Prior to addition to the fermentation medium, the stock solution was autoclaved at 121 °C for 20 min.

Acid-heat pretreatment protocol by Abol-Fotouh *et al.* (2020) was executed to prepare sugarcane molasses (SM) solution. The SM solution was diluted 2-fold (w/v) with distilled water and centrifuged at 2580 xg for 20 min to eliminate solid materials. The supernatant was collected and adjusted to pH 3.0 with 4N H_2SO_4. This was then heated for 20 min, kept at room temperature the following day, and centrifuged. The stock solution was labeled as TSM (treated sugarcane molasses) and stored at 4 °C.

Preparation of bacterial inoculum

The bacterial strain, *Komagataeibacter hansenii* RM-03 was locally isolated from rotten starfruit, and obtained from Microbial Culture Collection Unit (UniCC) at Universiti Putra Malaysia (UPM), Serdang. The inoculum was prepared by transferring one quadrant from agar into Hestrin-Schramm (HS) medium containing 20 g/ L glucose, 5 g/ L yeast extract, 5 g/ L peptone, 2.7 g/ L Na_2HPO_4, 1.15 g/ L citric acid and 1.5 % ethanol. It was shaken for 18 h at 30 °C in a shaking incubator before inoculation of 10 mL into 90 mL of liquid fermentation medium (Gomes *et al.* 2013 with modifications).

Biosynthesis and purification of BNC

The biosynthesis of BNC was done following the method described by Abol-Fotouh *et al.* (2020) with some modifications. The Hestrin-Schramm (HS) medium used as fermentation medium was formulated and modified by substituting glucose source with 2 % (v/v) of each 3 stock solutions (TSM, BPW, PPW). The medium was adjusted to pH 5.5 using 1.0 M CH_3COOH. Then, 10 mL of *K. hansenii* RM-03 inoculum was inoculated to each 90 mL of modified HS medium and fermented at 28 °C for 7 days under static condition. All the experiments were carried out in triplicate and under sterile conditions. The BNC pellicle produced on each surface medium was harvested and immersed separately in running water for 24 h. Each BNC pellicle was then incubated at 80 °C in 0.1 M NaOH solution to break down bacterial cells in the BNC (Abba *et al.*, 2018). The purified BNC pellicles were washed several times with distilled water and subjected for biosynthesis of BNC-Ag nanocomposite.

Analysis of sugar content in extracts

Total sugar of each prepared waste extract (TSM, BPW, PPW), as well as the initial sugar content and final sugar content of the fermentation medium were determined using phenol-sulphuric acid method by Nielsen (2010). A glucose standard curve was constructed prior to the analysis. All samples were diluted 2000-fold, before 0.05 mL of 80 % phenol was added. After mixing using a vortex machine, 5 mL sulphuric acid was added rapidly. All test tubes were left to stand for 10 min before being placed in a 25 °C water bath for another 10 min. The test tubes

were vortexed, and the solution was examined using UV-visible absorbance spectroscopy. Absorbance of the standard glucose solution and all the samples were read at 490 nm.

Preparation of M. charantia fruit extract

M. charantia fruit extract was prepared following the method described by Nahar *et al.* (2015) with some modifications. The fresh *M. charantia* (bitter gourd) fruits were washed several times with distilled water to remove the dust, cut into smaller pieces and dried in the oven at 120 °C for 24 h. The dried pieces were ground to fine powder using a commercial dry miller. About 30 g of *M. charantia* fruit powder was added in 300 mL distilled water and boiled for 45 min. Then mixture was filtered using muslin cloth and Whatman filter paper no. 40. The filtrate was denoted as *M. charantia* fruit extract to be used for the reduction of AgNP.

Phytochemical analysis of the M. charantia fruit extract

The phytochemical composition of prepared *M. charantia* fruit extract was done to examine the presence of major bioactive compounds such as alkaloids, saponins, phenolics, tannins, and flavonoids.

Screening of alkaloids

Firstly, 3 mL of *M. charantia* fruit extract was put into the test tube and 3 mL of concentrated H_2SO_4 was added. Next, a few drops of Wagner's reagent (2.5 g I_2 in 250 mL KI solution (5wt %) were added into the acidified extract. Red brown precipitate forms when there is presence of alkaloids (Nguyen *et al.*, 2020).

Screening of saponins

A frothing test was used to analyze the presence of saponins. 5 mL of *M. charantia* fruit extract was added into the test tube and was shaken for a few min. Saponins are present if the froth appears stable for more than 10 min (Nguyen *et al.*, 2020).

Screening of Phenolics and tannins

The 3 mL *M. charantia* fruit extract was added into the test tube followed by dropping 1 mL of $FeCl_3$ (5wt%). A bluish-black, blue- green colouration or precipitate will indicate the presence of tannins (Teketle & Kiros, 2020) while a blue, green, red or purple colour will be a positive test for phenolics (Rao, 2016).

Screening of Flavonoids

The *M. charantia* fruit extract (1 mL) was taken in a test tube and a few drops of dilute NaOH solution was added. An intense yellow colour will appear in the test tube. It became colourless when in addition to a few drops of dilute acid that indicated the presence of flavonoids (Hossain *et al.*, 2013).

Green synthesis of BNC-Ag nanocomposites

The BNC-Ag nanocomposite was prepared following the green method of Moniri *et al.* (2018). First, purified BNC pellicles were immersed in 1 mM of $AgNO_3$ to allow the dispersion of Ag ions. Then, 15 mL of *M. charantia* fruit extract was introduced as reducing agent, with constant stirring at 45 °C. The change in colour from bright yellow to dark brown indicated the formation of AgNP. The mixture was then ultrasonicated for 30 min. The reduction of Ag ions was monitored by measuring the UV-visible spectrum. 1 mL of the mixture sample was transferred into a cuvette and analyzed in different wavelengths from 400 to 600 nm at room temperature (Krithiga *et al.*, 2015). A solution of $AgNO_3$ was used as blank control. The synthesised BNC-Ag nanocomposite pellicle was subjected to further characterisation.

Characterisation of BNC-Ag nanocomposites

Field emission scanning electron microscopy (FESEM)

The BNC-Ag nanocomposite pellicle was dried to thin film, cut into a piece of about 3 x 3 mm, and mounted to SEM metal holder. The sample surface was sputtered by platinum, and viewed using FESEM (JSM-7600F, JEOL, Japan) with an accelerating voltage of 5 kV.

X-ray diffraction (XRD)

The BNC-Ag nanocomposite pellicle was dried to thin film and the crystallinity was determined with X-ray diffractometer with Cu Kα radiation (λ = 1.5405 Å) at 45 kV voltage and 40 mA current. The samples were scanned in 2θ range between 10° to 40° degrees (Mangayil *et al.*, 2017). The crystallinity index was calculated using the method described by (Segal *et al.,* 1959) as follows:

$$CrI\ (\%) = [\ I_{(200)} - I_{(am)} / I_{(200)}] \times 100]$$

Where I_{200} represents the intensity of (200) lattice diffraction at $2\theta = 22.9^{\circ}$, while I_{am} represents the intensity of the amorphous region at $2\theta = 18^{\circ}$ (Pacheco *et al.,* 2017; Segal *et al.,* 1959).

Fourier-transform infrared spectroscopy (FTIR)

The BNC-Ag nanocomposite pellicle was dried to thin film, and analyzed using Fourier-transform infrared spectrophotometer at 4 cm^{-1} resolution and spectra range from 4000 to 400 cm^{-1} (Abol-Fotouh *et al.,* 2020).

Antibacterial activity of BNC-Ag nanocomposite

BNC-Ag nanocomposites were screened for antibacterial activity test against gram-positive (*Bacillus subtilis* and *Staphylococcus aureus)* and gram-negative bacteria (*Pseudomonas aeruginosa* and *Salmonella typhi)* obtained from the laboratory stock culture at Universiti Putra Malaysia. All the bacterial strains were pathogens except for *B. subtilis*. The selection of bacteria in the antibacterial activity test aimed to evaluate the efficacy of the synthesised AgNPs in combating these disease-causing bacteria, especially those demonstrating resistance to multiple antibiotic types.

The disk diffusion method was employed, following the procedure outlined by Moniri *et al.* (2018). In this method, a standardized amount of bacterial culture is spread onto the surface of agar plates. Muller-Hinton agar, a common medium for antibiotic susceptibility testing, was prepared for the experiment. 100 µL of the bacterial cultures were inoculated onto the Muller-Hinton agar. Dried and autoclaved BNC-Ag nanocomposite films with a diameter of 1.5 mm were placed onto the agar. The BNC film with incorporation of commercial silver ion was used as positive control while BNC film without any incorporation was used as a negative control. The agar plates were then incubated overnight at 37 °C. This incubation period allows the bacteria to grow and form colonies. After incubation, the zones of inhibition were measured as an average of three independent experiments, indicating the reproducibility of the results.

RESULTS AND DISCUSSION

Biosynthesis of BNC on different agricultural waste substrates in HS medium

This research was conducted by substituting the glucose source in the Hestrin Schramm medium with 2 % (v/v) of various agricultural wastes stock solution; namely, treated sugarcane molasses (TSM), banana peel waste (BPW) and pineapple peel waste (PPW). All samples were incubated under static condition for 7 days at 28 °C.

Results showed significantly higher BNC yields than previous research, especially with TSM-HS medium reaching 8.19 g/L in just 7 days, surpassing other reported values (Table 1). For context, Rodrigues *et al.* (2019) reported a BNC yield of about 7.5 g/L on a mixture of ethanol and sugarcane molasses after a 9-day cultivation period, while Abol-Fatouh *et al.* (2020) achieved 3.9 g/L of BNC on molasses-HS medium in the same 7-day timeframe. The efficient BNC production is believed to be largely attributed to the remarkable capability displayed by K. hansenii RM-03, a member of the Komagataeibacter genus known for being an efficient producer of BNC (Przygrodzka *et al.*, 2022; Ryngajłło *et al.,* 2020). To date, K. hansenii HUM-1 strain employs a special genetic code to arrange their cells in a unique way, creating an ultrafine, strong, and biocompatible cellulose structure (Pfeffer *et al.,* 2017). For other modified media like BPW-HS and PPW-HS, the BNC yield was comparable to previous studies, generally around 2.5 g/L. A study by Castro *et al.* (2011) reported 2.8 g/L of BNC production by G. swingsii on pineapple peel juice medium after 13 days of static cultivation.

Green synthesis AgNP by M. charantia fruit extract

AgNPs were synthesised using $AgNO_3$ as the precursor of Ag, and M. charantia fruit extract as the reducing and capping agent. The phytochemical constituents of the M. charantia extract were qualitatively analyzed. Based on the screening, M. charantia fruit extracts indicated the presence of alkaloids, saponins, flavonoids, phenol and tannins. These phytochemicals are reported to be responsible for the reduction of Ag^{+} to AgNP (Bawazeer *et al.*, 2021). Some of

them have known health-promoting properties, such as phenols for antioxidants and flavonoids for anti-inflammatory (Lavanya and Ambikapathy, 2016). The phytoconstituents found in plants serve as stabilizing or capping agents, preventing agglomeration, controlling particle size, facilitating biofunctionalization, and imparting stability to AgNPs. As per David *et al.* (2014), the primary phytochemical in the extract of M. charantia leaves, particularly involved in the reduction of Ag ions, is phenol. According to the study, Ag ions can create intermediate complexes with the phenolic OH groups present in gallic acid. Subsequently, these complexes undergo oxidation to the quinone form, leading to the reduction of Ag+ to AgNPs. Furthermore, the quinoid compound generated during the oxidation of phenolic groups can adhere to the nanoparticle surface, playing a crucial role in stabilizing their suspension (David *et al.,* 2014).

In this study, AgNP synthesised using M. charantia fruit extract incorporated into BNC was aimed to impart antibacterial properties. A UV-visible spectroscopy was used to verify the reduction of AgNP. Following the addition of the M. charantia fruit extracts into 1 mM $AgNO_3$, the color of solution changed to dark brown. The UV-visible absorbance spectra showed maximum absorbance at 410 nm, which increased with M. charantia fruit extract concentrations (2.5, 5, 10, 15 mL) (Figure 1). A higher concentration of M. charantia fruit extract showed a sharper peak and stronger absorbance at 410 nm. To compare the difference between synthesised AgNPs and $AgNO_3$, the absorbance of $AgNO_3$ was also examined. In Figure 2, the sharp peak was observed at 290 to 300 nm and there was no peak absorption at 400 to 410 nm, which indicates there was no AgNPs present in the $AgNO_3$. Similar results have been reported by Oves *et al.* (2013).

Table 1 The production yield of BNC on modified HS-media of (TSM-HS), (BPW-HS) and (PPW-HS) and (HS) after 7 days of cultivation by *K. hansenii* RM-03. (Si) Initial total sugar concentration; (Sf) Final total sugar concentration; (α) Substrate conversion ratio; (Y) Yield of BNC products; (R) rate of BNC production.

Media	Si (g/L)	Sf (g/L)	α (%)	Y (g/L)	R
TSM-HS	10.7	7.1	33.64	8.19	0.050
BPW-HS	3.7	2.4	35.14	2.11	0.013
PPW-HS	2.9	2.1	27.58	2.16	0.013
HS	21.24	13.93	34.41	2.33	0.014

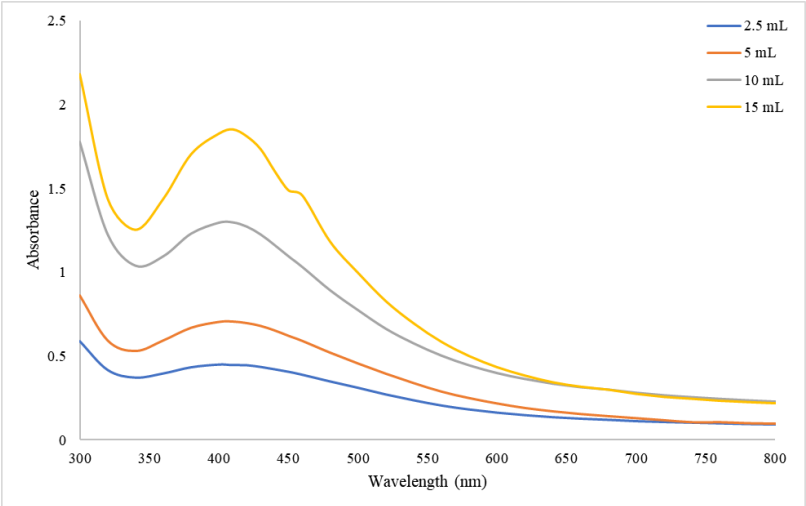

Figure 1 UV-visible absorption spectra of AgNP synthesised at different concentrations of *M. charantia* fruit extract (2.5, 5, 10, 15 mL).

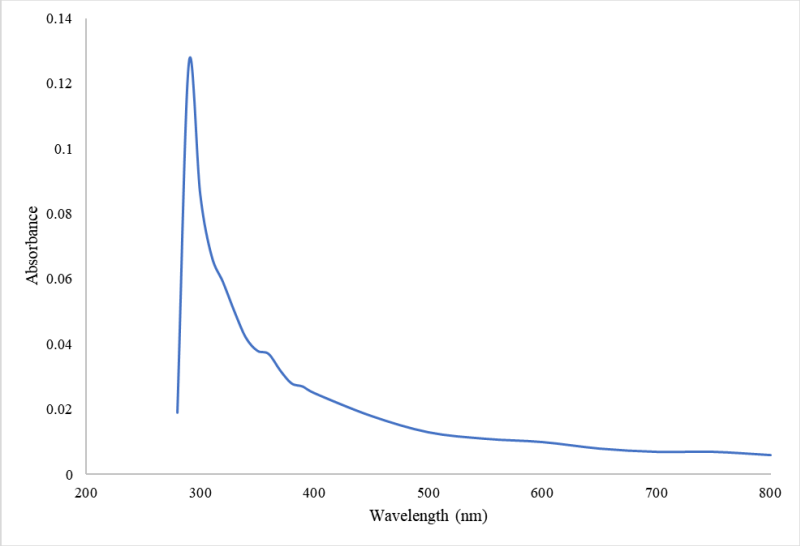

Figure 2 UV-visible absorption spectra of 1 mM $AgNO_3$

Morphological characterisation by FESEM and TEM

BNC synthesised using different agricultural wastes were purified separately (Figure 3A-D) and then incorporated with AgNP using M. charantia fruit extract (Figure 3E-H). Each BNC sample was in the form of dried film, and the surface morphology was observed via FESEM. As per observation, upon incorporation, the Ag^+ ions effectively adsorbed into BNC fibres, distributing themselves throughout the network of cellulose microfibrils due to the attractive forces between the positively charged Ag+ ions and the negatively charged hydroxyl groups on the BNC molecules (He *et al*., 2003). The localization of Ag within the BNC fibres was further confirmed by detection using energy dispersive x-ray spectroscopy (EDX) through mapping across the area (Figure 4). The EDX spectrum revealed major energy peaks corresponding to C, K and Ag.

Figure 5 showed that the BNC exhibited an elongated ribbon structure that appeared intertwined with each other. Zooming in at a magnification of 100000x, the micrograph exhibits a combination of isolated single strands and bundled ribbons of BNC. The individual strands of BNC ribbons appear to have noticeably more spaces between each strand. There are also individual AgNP with a size of less than 20 nm adhere to the BNC fibre as a single nanoparticle distributed evenly across the BNC surface. In some cases, the particles tend to interact with one another due to the high surface area per unit mass, leading to agglomeration (Ju-Nam and Lead, 2008). This can be resolved if a capping agent, which acts as a charge stabilizer, is present. In this study, M. charantia fruit extract plays a role as capping agent preventing the nanoparticles from clumping together, which is desirable for the characteristics of nanocomposite materials. In addition, agglomerated AgNP is often perceived to negatively impact the properties of nanocomposite such as weak tensile strength (Ashraf *et al.,* 2018). Therefore, it is necessary for AgNP to be evenly distributed by the presence of a good capping agent.

Structural characterisation by XRD

Structural characterisation was made to investigate the effect of utilising different agricultural waste substrates on the membrane of BNC before and after incorporation with AgNP. The results of XRD analysis were shown in Figure 6. The BNC products generally have three main peaks at a diffraction angle of 14.25°, 16.42° and 22.45° that are corresponding to the semicrystalline planes of (100), (010) and (110), respectively. In this study, there are variations in the crystallinity index of BNC when employing different agricultural waste substrates and after incorporation of AgNP, implying that varied carbon sources have a direct impact on the BNC crystallinity.

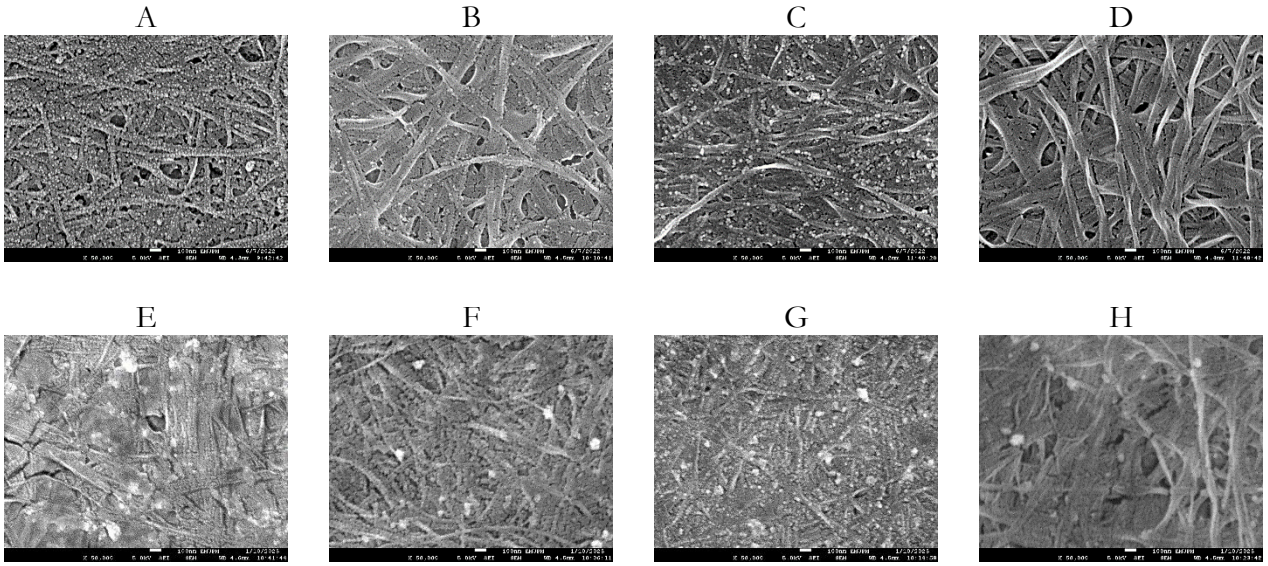

Figure 3 FESEM of BNC before incorporation (A) TSM-HS, (B) BPW-HS, (C) PPW-HS, (D) HS, and after incorporation with AgNP (E) TSM-AgNP, (F) BPW-AgNP, (G) PPW-AgNP, (H) HS-AgNP.

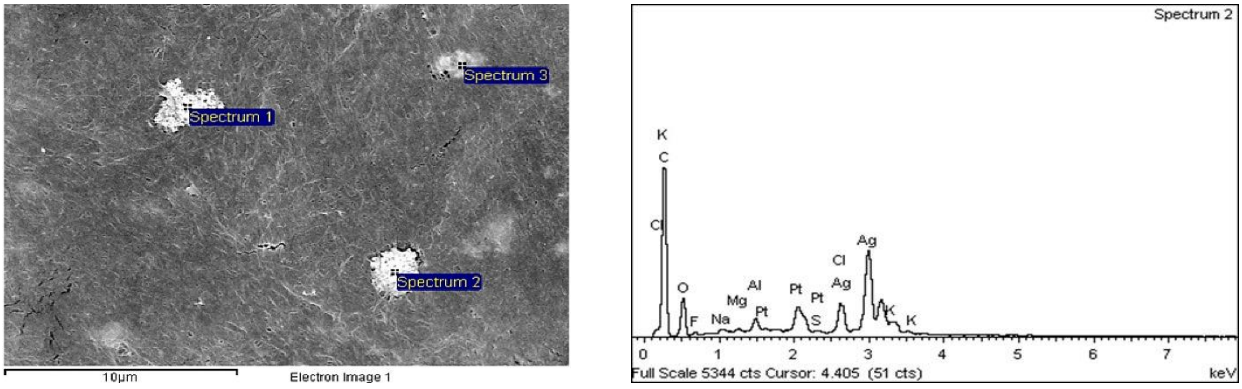

Figure 4 EDX analysis of BNC-Ag nanocomposite.

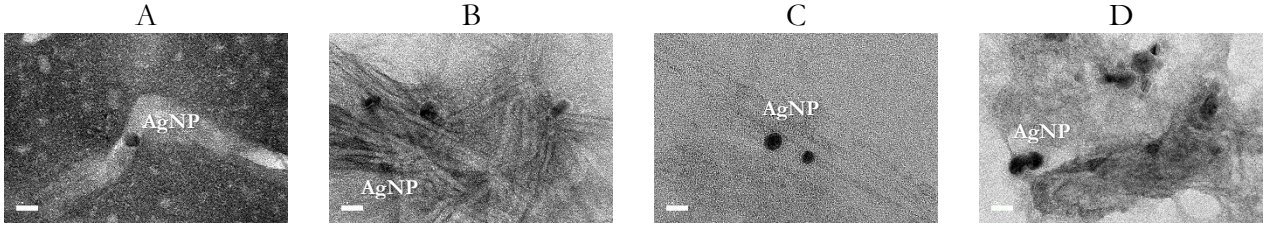

Figure 5 TEM of BNC-Ag nanocomposite (A) TSM-AgNP, (B) BPW-AgNP, (C) PPW-AgNP, (D) HS-AgNP which AgNPs appeared as dark spherical particles.

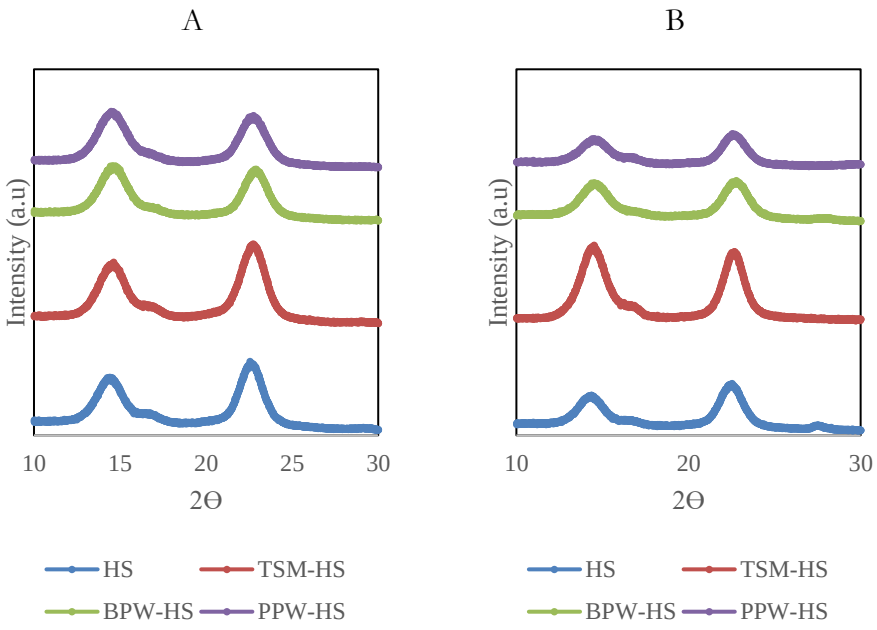

Figure 6 X-ray diffraction pattern of the (A) BNC and (B) BNC-Ag nanocomposites produced by *K. hansenii* RM-03 on (TSM-HS), (BPW-HS), (PPW-HS), and (HS) medium.

The highest CrI was recorded on BNC produced on TSM-HS (84.78%), which was slightly higher than control HS medium (83.78%). Meanwhile, lower CrI was recorded on BNC produced on BPW-HS (81.52%) and PPW-HS (79.59%). Besides, we observed a slight decrease in crystallinity on all BNC products after incorporation of AgNP, postulating that incorporation AgNP alters the crystallinity of BNC. Table 2 summarizes the CrI (%) of BNC produced on different agricultural waste substrates before and after incorporation of AgNP.

Table 2 Crystallinity index (CrI) of the BNC synthesised by *K. hansenii* RM-03 culturing on (PPW-HS), (BPW-HS), (TSM-HS) and (HS) media.

Medium	CrI (%) before incorporation of AgNP	CrI (%) after incorporation of AgNP
PPW-HS	79.59	75.99
BPW-HS	81.52	79.45
TSM-HS	84.78	84.38
HS	83.58	81.53

Functional group characterisation by FTIR

FTIR spectroscopy is used to examine the chemical composition and identify functional groups present in a material. Figure 7 displays the FTIR spectra obtained in the bacterial nanocellulose. Upon examination at spectra ranging from 650 to 4000 cm^{-1} , there were five major peaks that emerged consistently across all of the BNC samples. It is challenging to determine the exact type of cellulose solely based on IR spectra. However, the consistent appearance of major peaks suggests that the BNC samples contain cellulose or cellulose-like compounds with similar chemical compositions. The broad peak observed at 3200 to 3600 cm^{-1} is attributed to the stretching vibrations of O-H bonds, which are characteristic of the alcohol functional group commonly found in BNC (Abol-Fatouh *et al.*, 2020; Apriyana *et al.*, 2020). Another common peak is near 2900 cm^{-1} known for the C-H stretch. Meanwhile, another peak at around 1600 cm^{-1} indicates the C=C stretch. This suggests that varying the carbon source and incorporation of AgNP had no significant effect on the functional groups and it did not introduce noticeable changes in the overall composition of the BNC. This discovery aligns with a study reported by Abol-Fatouh *et al.* (2020).

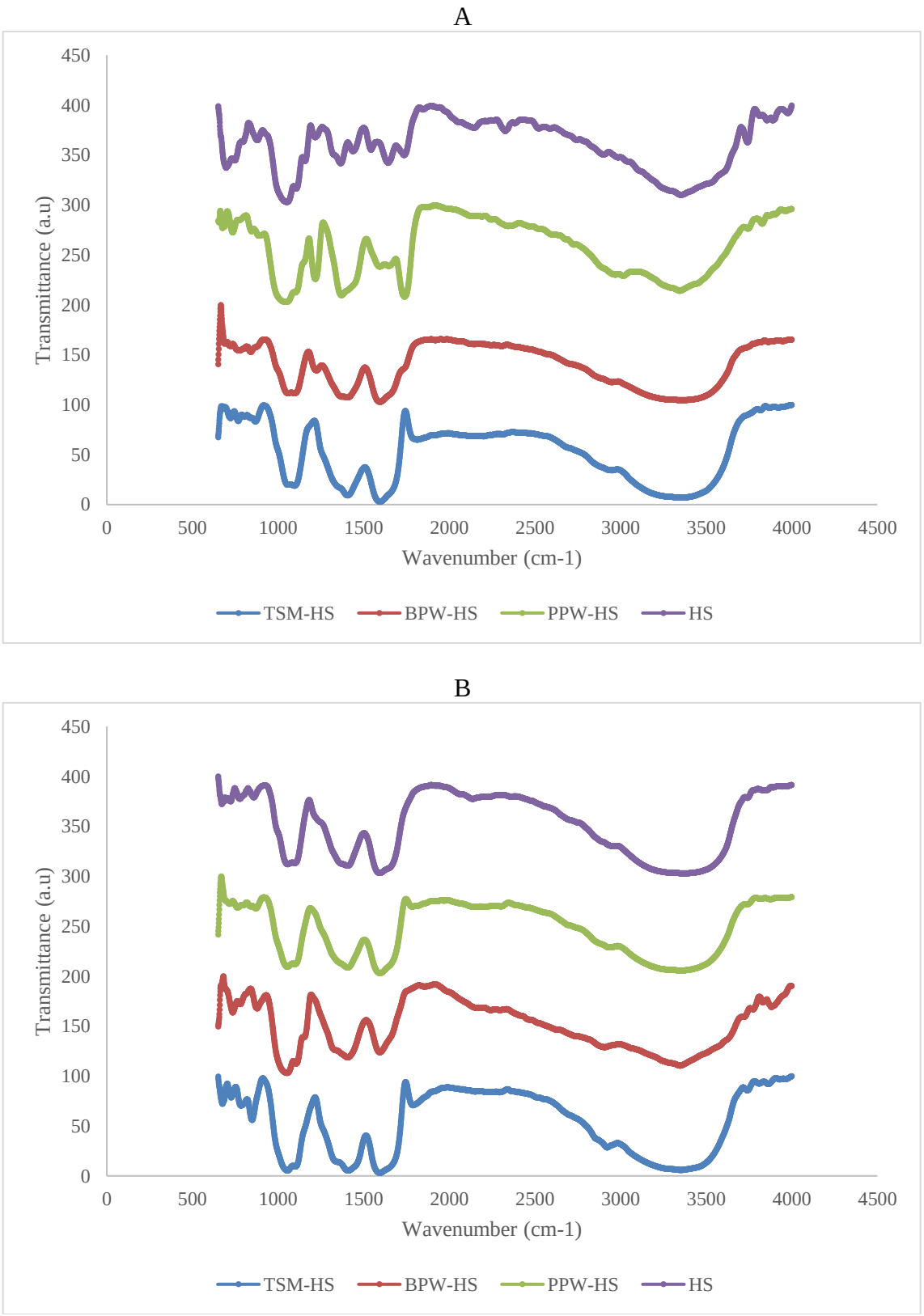

Figure 7 FTIR spectra of the BNC (A) and BNC-Ag nanocomposites (B) produced by *K. hansenii* RM-03 on (TSM-HS), (BPW-HS), (PPW-HS), and (HS) medium.

Antibacterial activity of BNC-Ag nanocomposites

The synthesised BNC-Ag nanocomposites were observed on its antibacterial activity via disc diffusion method. Table 3 summarizes the diameter zone of inhibition for the four bacterial strains. As can be seen in Figure 8, the overall inhibition zone for *B. subtilis* in different BNC samples grown on different media was the highest in comparison to the other three bacterial strains. *S. aureus* has the lowest bactericidal effects with 6.7 mm zone of inhibition. The remaining bacterial strains: *P. aeruginosa* and *S. typhi* showed nearly the same antibacterial activity with diameter of zone of inhibition lies between 8.5 to 11.0 mm. In this study as well, pure BNC without the incorporation of AgNP as a negative control did not display a zone of inhibition (Figure 9). The absence of antibacterial properties in the pure BNC sample supports the notion that the successful incorporation of AgNP is responsible for introducing antibacterial activity to the BNC.

The gram-positive bacteria: *S. aureus* appears to be less sensitive compared to gram negative bacteria *P. aeruginosa* and *S. typhi*. The increased sensitivity of gram-negative bacteria towards AgNPs can be attributed to the presence of negatively charged lipopolysaccharide molecules that coat their outer membrane. These molecules have a strong affinity for the positive ions released by most AgNPs, leading to their accumulation and increased uptake within the bacterial cells. This accumulation eventually results in intracellular damage (Slavin *et al.,* 2017). However, the specific behaviour of individual bacteria can vary, as demonstrated by the unique response of gram-positive *B. subtilis* to the BNC-Ag nanocomposite.

Table 3 Diameter of inhibition zone of synthesised BNC-Ag nanocomposite against *B. subtilis, S. aureus, P. aeruginosa* and *S. typhi.*

Bacteria	Mean diameter of inhibition zone (mm)				
	TSM-AgNP	**BPW-AgNP**	**PPW-AgNP**	**HS-AGNP**	**Commercial Silver ion**
Bacillus subtilis	12.0	11.0	11	11.0	15.2
Staphylococcus aureus	6.7	7.0	8.8	8.8	16.8
Pseudomonas aeruginosa	8.5	9.0	9.0	9.0	16.8
Salmonella typhi	11.0	9.8	10.0	11.0	14.8

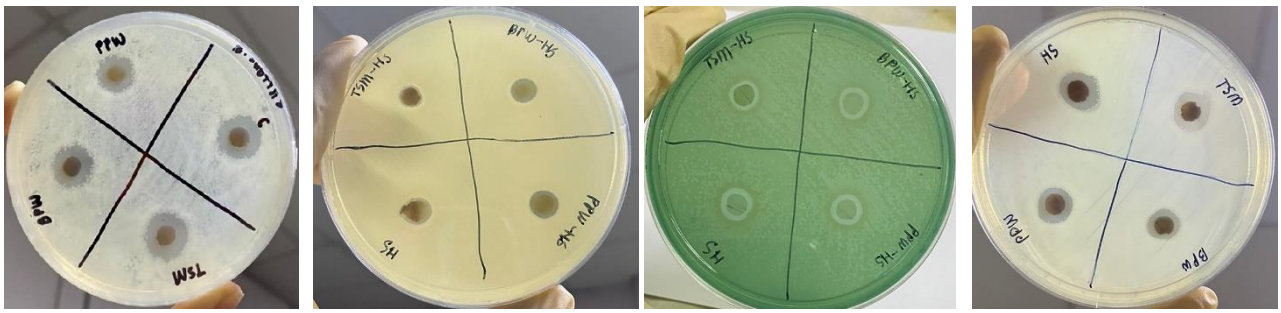

A B C D

Figure 8 Zone of inhibition of BNC-Ag nanocomposite against (A) *B. subtilis*, (B) *S. aureus*, (C) *P. aeruginosa*, (D) *S. typhi* in BNC sample on each culture medium.

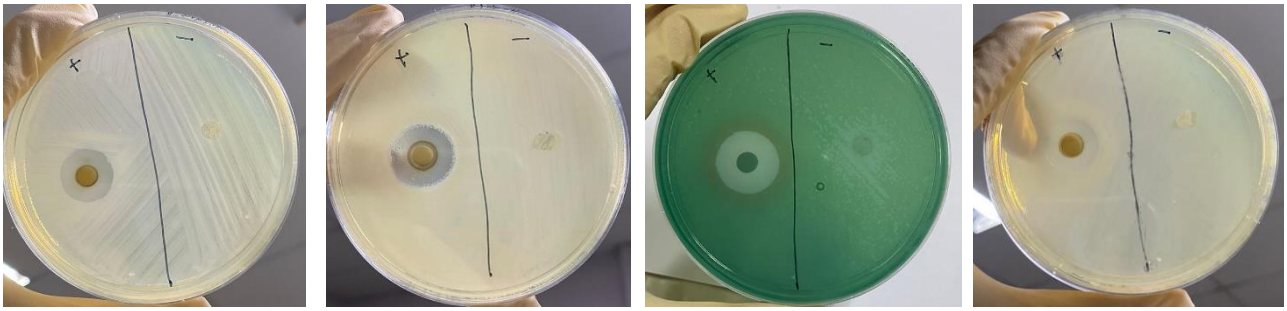

A B C D

Figure 9 Zone of inhibition of BNC-Ag nanocomposite on (A) *B. subtillis*, (B) *S. aureus*, (C) *P. aeruginosa,* (D) *S. typhi* in commercial silver ion (positive control) and pure BNC (negative control).

CONCLUSION

In this study, BNC was successfully synthesised using *K. hansenii* RM-03 with agricultural wastes as the carbon source. Among the tested carbon sources, TSM-HS medium exhibited the highest BNC concentration at 8.19 g/L. The incorporation of BNC with AgNP synthesised using *M. charantia* fruit extract was also achieved. The results obtained from FESEM and TEM showed similar nanofibre sizes across different carbon sources, while slight variations in crystallinity index were observed in XRD analysis. Furthermore, FTIR analysis indicated an identical chemical profile assigned to typical cellulose type in all BNC-Ag nanocomposites.

Remarkably, all BNC-Ag nanocomposites exhibited excellent antibacterial activity against both gram-positive and gram-negative bacteria. This finding highlights the potential of BNC-Ag nanocomposites as effective antibacterial materials. The antibacterial activity demonstrated the capability of BNC-Ag nanocomposites to protect against bacterial infections, suggesting their potential application in wound dressing.

The study also shed light on the promising use of agricultural wastes as an alternative carbon source for BNC synthesis in HS medium. This finding opens new avenues for utilising sustainable and cost-effective carbon sources, reducing reliance on conventional carbon sources and promoting environmentally friendly approaches in BNC production. Further research and development in this field could lead to the advancement of wound care technologies and the production of more efficient and accessible antibacterial materials.

ACKNOWLEDGEMENTS

We would like to acknowledge Universiti Putra Malaysia for the financial support under the Inisiatif Putra Siswazah (IPS) 9704900.

CONFLICT OF INTEREST

The authors have declared that no conflict of interest exists.

REFERENCES

Abba, M., Abdullahi, M., Nor, M. H. M., Chong, C. S., & Ibrahim, Z. 2018. Isolation and characterisation of locally isolated *Gluconacetobacter xylinus* BCZM sp. with nanocellulose producing potentials. *IET Nanobiotechnology*, *12*(1), 52-56.

Abol-Fotouh, D., Hassan, M. A., Shokry, H., Roig, A., Azab, M. S., & Kashyout, A. E. H. B. 2020. Bacterial nanocellulose from agro-industrial wastes: Low-cost and enhanced production by *Komagataeibacter saccharivorans* MD1. *Scientific Reports*, *10*(1), 1-14.

Apriyana, A. Y., Andriani, D., & Karina, M. 2020. Production of bacterial cellulose from tofu liquid waste and rice-washed water: Morphological property and its functional groups analysis. In *IOP Conference Series: Earth and Environmental Science* (Vol. 483, No. 1, p. 012005). IOP Publishing.

Ashraf, M. A., Peng, W., Zare, Y., & Rhee, K. Y. 2018. Effects of size and aggregation/agglomeration of nanoparticles on the interfacial/interphase properties and tensile strength of polymer nanocomposites. *Nanoscale Research Letters*, *13*(1), 1-7.

Barja, F. 2021. Bacterial nanocellulose production and biomedical applications. *Journal of Biomedical Research*, *35*(4), 310.

Bawazeer, S., Rauf, A., Shah, S. U. A., Shawky, A. M., Al-Awthan, Y. S., Bahattab, O. S., ... & El-Esawi, M. A. 2021. Green synthesis of silver nanoparticles using *Tropaeolum majus*: Phytochemical screening and antibacterial studies. *Green Processing and Synthesis*, *10*(1), 85-94.

Bortolotti, M., Mercatelli, D., & Polito, L. 2019. *Momordica*

charantia, a nutraceutical approach for inflammatory related diseases. *Frontiers in Pharmacology*, *10*, 486.

Castro, C., Zuluaga, R., Putaux, J. L., Caro, G., Mondragon, I., & Gañán, P. 2011. Structural characterization of bacterial cellulose produced by *Gluconacetobacter swingsii* sp. from Colombian agroindustrial wastes. *Carbohydrate Polymers*, *84* (1), 96-102.

Dandawate, P. R., Subramaniam, D., Padhye, S. B., & Anant, S. 2016. Bitter melon: A panacea for inflammation and cancer. *Chinese Journal of Natural Medicines*, *14*(2), 81-100.

David, S. A., Ponvel, K. M., Fathima, M. A., Anita, S., Ashli, J., & Athilakshmi, A. 2014. Biosynthesis of silver nanoparticles by *Momordica charantia* leaf extract: Characterization and their antimicrobial activities. *Journal of Natural Product and Plant Resources*, *4*(6), 1-8.

Gomes, F. P., Silva, N. H., Trovatti, E., Serafim, L. S., Duarte, M. F., Silvestre, A. J., ... & Freire, C. S. 2013. Production of bacterial cellulose *by Gluconacetobacter sacchari* using dry olive mill residue. *Biomass and Bioenergy*, *55*, 205-211.

He, J., Kunitake, T., & Nakao, A. 2003. Facile in situ synthesis of noble metal nanoparticles in porous cellulose fibres. *Chemistry of Materials*, *15*(23), 4401-4406.

Hossain, M. A., AL-Raqmi, K. A. S., AL-Mijizy, Z. H., Weli, A. M., & Al-Riyami, Q. 2013. Study of total phenol, flavonoids contents and phytochemical screening of various leaves crude extracts of locally grown Thymus vulgaris. *Asian Pacific Journal of Tropical Biomedicine*, *3*(9), 705–710.

International Organization for Standardization. 2023. *Nanotechnologies – Vocabulary for cellulose nanomaterial* (ISO/TS Standard No. 20477). Retrieved from https:// www.iso.org/obp/ui/en /#iso:std:83010:en

Jozala, A. F., de Lencastre-Novaes, L. C., Lopes, A. M., de Carvalho Santos-Ebinuma, V., Mazzola, P. G., Pessoa-Jr, A., ... & Chaud, M. V. 2016. Bacterial nanocellulose production and application: A 10-year overview. *Applied Microbiology and Biotechnology*, *100*(5), 2063-2072.

Ju-Nam, Y., & Lead, J. R. 2008. Manufactured nanoparticles: An overview of their chemistry, interactions and potential environmental implications. *Science of the Total Environment*, *400*(1-3), 396-414.

Khan, H., Saroha, V., Raghuvanshi, S., Bharti, A. K., & Dutt, D. 2021. Valorization of fruit processing waste to produce high value-added bacterial nanocellulose by a novel strain *Komagataeibacter xylinus* IITR DKH20. *Carbohydrate Polymers*, *260*, 117807.

Krithiga, N., Rajalakshmi, A., & Jayachitra, A. 2015. Green synthesis of silver nanoparticles using leaf extracts of *Clitoria ternatea* and *Solanum nigrum* and study of its antibacterial effect against common nosocomial pathogens. *Journal of Nanoscience*, *2015*.

Lavanya, A., & Ambikapathy, V. 2016. Preliminary qualitative analysis of phytoconstituents of *Dichrostachys cinerea L. Journal of Pharmacognosy and Phytochemistry*, *5*(3), 86.

Lin, N., & Dufresne, A. 2014. Nanocellulose in biomedicine: Current status and future prospect. *European Polymer Journal*, *59*, 302-325.

Maneerung, T., Tokura, S., & Rujiravanit, R. 2008. Impregnation of silver nanoparticles into bacterial cellulose for antimicrobial wound dressing. *Carbohydrate Polymers*, *72*(1), 43-51.

Mangayil, R., Rajala, S., Pammo, A., Sarlin, E., Luo, J., Santala, V., ... & Tuukkanen, S. 2017. Engineering and characterization of bacterial nanocellulose films as low cost and flexible sensor material. *ACS Applied Materials & Interfaces*, *9*(22), 19048-19056.

Masum, M. M. I., Siddiqa, M. M., Ali, K. A., Zhang, Y., Abdallah, Y., Ibrahim, E., ... & Li, B. 2019. Biogenic synthesis of silver nanoparticles using *Phyllanthus emblica* fruit extract and its inhibitory action against the pathogen *Acidovorax oryzae* strain RS-2 of rice bacterial brown stripe. *Frontiers in Microbiology*, *10*, 820.

Moniri, M., Moghaddam, A. B., Azizi, S., Rahim, R. A., Zuhainis, S. W., Navaderi, M., & Mohamad, R. 2018. In vitro molecular study of wound healing using biosynthesised bacteria nanocellulose/silver nanocomposite assisted by bioinformatics databases. *International Journal of Nanomedicine*, *13*, 5097.

Nahar, M. K., Zakaria, Z., Hashim, U., & Bari, M. F. 2015. Green synthesis of silver nanoparticles using *Momordica charantia* fruit extracts. In *Advanced Materials Research* (Vol. 1109, pp. 35-39). Trans Tech Publications Ltd.

Naveed, M., Bukhari, B., Aziz, T., Zaib, S., Mansoor, M. A., Khan, A. A., ... & Alhomrani, M. 2022. Green synthesis of silver nanoparticles using the plant extract of *Acer oblongifolium* and study of its antibacterial and antiproliferative activity via mathematical approaches. *Molecules*, *27*(13), 4226.

Nguyen, D. H., Vo, T. N. N., Nguyen, N. T., Ching, Y. C., & Hoang Thi, T. T. 2020. Comparison of biogenic silver nanoparticles formed by *Momordica charantia* and *Psidium guajava* leaf extract and antifungal evaluation. *PLoS One*, *15*(9), e0239360.

Nielsen, S. S. 2010. Phenol-sulfuric acid method for total carbohydrates. In *Food Analysis Laboratory Manual* (pp. 47-53). Springer, Boston, MA.

Oves, M., Khan, M. S., Zaidi, A., Ahmed, A. S., Ahmed, F., Ahmad, E., ... & Azam, A. 2013. Antibacterial and cytotoxic efficacy of extracellular silver nanoparticles biofabricated from chromium reducing novel OS4 strain of *Stenotrophomonas maltophilia*. *PloS one*, *8*(3), e59140.

Pacheco, G., Nogueira, C. R., Meneguin, A. B., Trovatti, E., Silva, M. C. C., Machado, R. T. A., Ribeiro, S.J.L., da Silve Filho, E.C. and da S. Barud, H. 2017. Development and characterisation of bacterial cellulose produced by cashew tree residues as alternative carbon source. *Industrial Crops and Products*, *107*(May), 13–19.

Pfeffer, S., Santos, R., Ebels, M., Bordbar, D., & Brown Jr, R. M. 2017. Complete genome sequence of *Komagataeibacter hansenii* strain HUM-1. *Genome Announcements*, *5*(15), 10-1128.

Prabhu, S., & Poulose, E. K. 2012. Silver nanoparticles: Mechanism of antimicrobial action, synthesis, medical applications, and toxicity effects. *International Nano Letters*, *2* (1), 1-10.

Przygrodzka, K., Chareza, M., Banaszek, A., Zielińska, B., Ekiert, E., & Drozd, R. 2022. Bacterial cellulose production by *Komagateibacter xylinus* with the use of enzyme-degraded oligo-and polysaccharides as the substrates. *Applied Sciences*, *12*(24), 12673.

Rao, U. M. 2016. Phytochemical screening, total flavonoid and phenolic content assays of various solvent extracts of tepal of *Musa paradisiaca*. *Malaysian Journal of Analytical Science*, *20*(5), 1181–1190.

Rodrigues, A. C., Fontão, A. I., Coelho, A., Leal, M., da Silva, F. A. S., Wan, Y., ... & Gama, M. 2019. Response surface statistical optimization of bacterial nanocellulose fermentation in static culture using a low-cost medium. *New Biotechnology*, 49, 19-27.

Ross, P., Mayer, R., & Benziman, M. 1991. Cellulose biosynthesis and function in bacteria. *Microbiological Reviews*, *55*(1), 35-58.

Ryngajłło, M., Jacek, P., Cielecka, I., Kalinowska, H., & Bielecki, S. 2019. Effect of ethanol supplementation on the transcriptional landscape of bionanocellulose producer *Komagataeibacter xylinus* E25. *Applied Microbiology and Biotechnology*, *103*, 6673-6688.

Segal, L., Creely, J. J., Martin, A. E., and Conrad, C. M. 1959. An empirical method for estimating the degree of crystallinity

of native cellulose using the X-ray diffractometer. *Textile Research Journal*, *29*(10), 786–794.

Singh, V., Haque, S., Niwas, R., Srivastava, A., Pasupuleti, M., & Tripathi, C. 2017. Strategies for fermentation medium optimization: An in-depth review. *Frontiers in Microbiology*, *7*, 2087.

Slavin, Y. N., Asnis, J., Häfeli, U. O., & Bach, H. 2017. Metal nanoparticles: Understanding the mechanisms behind antibacterial activity. *Journal of Nanobiotechnology*, *15*(1).

Teketle, S., & Kiros, T. 2020. Effect of extraction solvent on qualitative and quantitative analysis of major phyto-constituents and *in-vitro* antioxidant activity evaluation of *Cadaba rotundifolia* Forssk leaf extracts. *Cogent Food and Agriculture*, *6*(1), 1853867.

Trache, D., Tarchoun, A. F., Derradji, M., Hamidon, T. S., Masruchin, N., Brosse, N., & Hussin, M. H. 2020. Nanocellulose: From fundamentals to advanced applications. *Frontiers in Chemistry*, *8*, 392.

Yahya, E. B., Elarbash, S. S., Bairwan, R. D., Mohamed, M. M. I., Khan, N. B., Harlina, P. W., & Abdul Khalil, H. P. S. 2023. The role of microorganisms in the isolation of nanocellulose from plant biomass. *Forests*, *14*(7), 1457.

Zhang, J., & Greasham, R. 1999. Chemically defined media for commercial fermentations. *Applied Microbiology and Biotechnology*, *51*, 407-421.

Zhang, X. F., Liu, Z. G., Shen, W., & Gurunathan, S. 2016. Silver nanoparticles: Synthesis, characterization, properties, applications, and therapeutic approaches. *International Journal of Molecular Sciences*, *17*(9), 1534.